Hindawi
International Journal of Polymer Science
Volume 2022, Article ID 2426749, 15 pages
https://doi.org/10.1155/2022/2426749

Research Article

N-Doped Graphene Quantum Dot Nanoparticle Synthesis of Optical Active Thermal Stable Polyurea Nanocomposites Using Polybutadiene Chain Modification

Zahra Rahmatpanah, Mir Mohammad Alavi Nikje, and Maryam Dargahi

Department of Chemistry, Faculty of Science, Imam Khomeini International University, Qazvin 34148-96818, Iran

Correspondence should be addressed to Mir Mohammad Alavi Nikje; alavi@sci.ikiu.ac.ir

Received 20 June 2022; Revised 27 August 2022; Accepted 30 September 2022; Published 14 October 2022

Academic Editor: Zhonghua Peng

Copyright © 2022 Zahra Rahmatpanah et al. This is an open access article distributed under the Creative Commons Attribution License, which permits unrestricted use, distribution, and reproduction in any medium, provided the original work is properly cited.

Geminate thermal stability with optical characteristics is a moving forward achievement in the preparation of polybutadiene-based polyurea nanocomposites. In this regard, nitrogen-doped graphene quantum dots were synthesized from a one-pot hydrothermal reaction of citric acid with urea in an aqueous solution. An in situ polymerization approach was used for the synthesis of polyurea from the reaction of telechelic amine functionalized polybutadiene and toluene diisocyanate (TDI) in the presence of the DBTDL catalyst. Nanocomposites were prepared using 1–3 weight percent of graphene N-quantum dot nanoparticles in the polymer matrix. ^{1}H-NMR and FT-IR spectroscopy techniques elaborated successful synthesis of primary polymer binder, polyurea and nanocomposites. Thermal degradation and characteristics were investigated using the TGA/DTG and DSC methods; lower degradation rates with progressed thermal stabilities as well as proportionate thermal characteristics with wider thermal service range were obtained especially in 3 wt% nanocomposite. Optical behavior information of samples was studied using UV-vis absorption and photoluminescence (PL) spectrometers. EDX, SEM, and AFM techniques confirmed successful nanoparticle and nanocomposite synthesis with improved morphologic and topographic properties.

1. Introduction

Along with the petroleum and resin industry outreach, the variety of resin-based products as well as the amount of environmental pollution increased. Natural and synthetic rubbers, including polybutadiene (PB), polyisoprene (PI), and polyethylene/diene (EPDM), are the most practical polymers in tire, automobile, sport, building, resin shoes, and belt products and wastes at the same time. Over the last few decades, approximately 1.4 million tons of waste rubber is produced as a side product of resin factory development [1, 2]. Common ways of this "black garbage" disposal, namely piling up, burying, and incineration, are not so efficient to avoid ecosystem issues like vermin occupation, disease outbreak, and air pollution [3]. Direct addition of rubber in asphalt and blending with resins are other more reasonable approaches of waste rubber disposal [4].

Sulfur- or carbon dioxide-crosslinked, vulcanized or reinforced polybutadiene rubber with carbon black or silica in the tire industry belongs to the category of non-environmental materials, and it does not have not the ability to return to the ecological cycle spontaneously [5, 6]. So, it does not make sense to claim recycling retired polybutadiene rubber, at least until successful separation methods are innovated. Nevertheless, pure polybutadiene itself also face deficiencies in processability and can be more utilizable by chain modification. According to a common belief coming from the green chemistry point of view, production of applicable functionalized polymers using existing underused polymers has far greater advantages than synthesizing novel polymers from new monomers. Likewise, chemical modification of the polybutadiene chain can be adopted with the aim of raising polymer application, creating functional polymers, refraining from the production of low use and

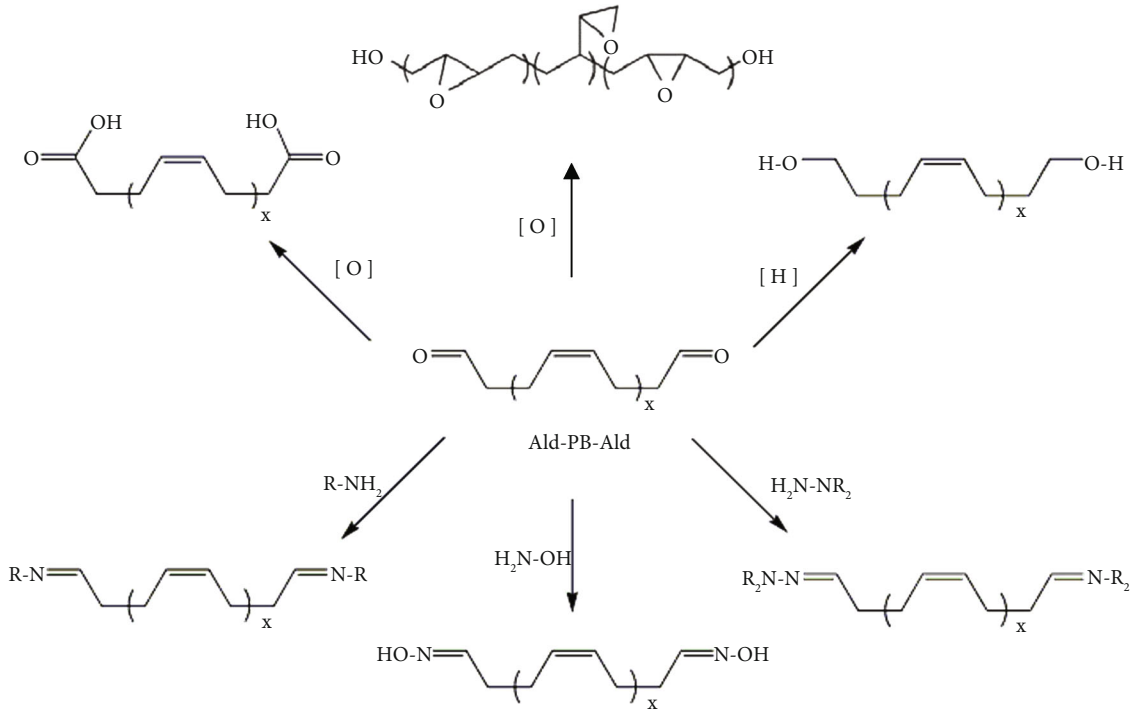

Scheme 1: Synthesizable functional groups from the terminal aldehyde group of polybutadiene.

polluting polymers, and also with an optimistic outlook of recycling these kinds of resins in the near future [7–9].

Chemical modification of the polybutadiene chain usually initiates with polymer backbone cutting processes like chemical degradation, metathesis, and ozonolysis, resulting in an aldehyde-functionalized polybutadiene. Terminal aldehyde functional groups are unique intermediates in synthesis of a collection of high-performance telechelic polymers by transforming to functional groups, including hydroxyl groups [10], epoxy [11], amine [12], carboxy [13], urea [14, 15], and urethane [16, 17], through known organic reactions (Scheme 1).

Ekinov and Onushchenko reported a blue-shift in the optic spectrum of CuCl nanoparticles in silica glass in 1981. Rosetti and coworkers' artwork in 1991 discussed the color change in colloid semiconductor solutions. Both findings are evidence of quantum dot formation, which is a zero-dimension particle containing several electrons in divided energy levels. In comparison with primary generations of quantum dots, graphene quantum dots (GQD) or carbon quantum dots (CQD) overcome the lack of safety for human being and bring forward secured use in applications associated with human health like biomedical cell imaging.

Semiconducting feature adjustable with energy band gap is the most important characteristic of quantum dots. So, they also divulge incredible optic and electronic properties, which distinguish this carbon based sp^2 hybrid materials from other semiconductors [18, 19]. Top-down synthesis processes, bottom-up approach, chemical and sol-gel methods, microemulsion, hot-solution decomposition, and steam phase processes are the prevalent ways of GQD achievement over the last two decades [20, 21].

Quantum dot doping or alloying with metal elements are substantial approach to raising quantum dot application in opto-electronic, magnetic, biologic, and spintronic technologies. The structural defects (hole or electron) coming from doping processes called activators create turbulence in energy level arrays with local quantum state development, locate within band gaps, and bring forward brand-new optical properties [22]. Heretofore, varied elements including P, N, Na, B, and Li are employed in quantum dot doping.

Nitrogen-doped quantum dots have unique features like heat conducting, fluorescence, high surface area and biocompatibility, appropriate thermal/chemical resistance, and other particle size-dependent properties. Utilization of modified quantum dots in reinforcement of elastomers like polyurea wipes out the polymer mechanical deficiencies and provides most of the required beneficial properties and at the same time [23, 24].

In the pursuit of earlier reports about introduction of novel applicable polyurethane and polyurea nanocomposites [14, 16, 25, 26], we followed up the synthesis of an optical active nanocomposite using polybutadiene-based polyurea. There are a couple of novelties in the current manuscript. Using polybutadiene as a polyurea backbone, using quantum dots as nanocomposite filler, successful introduction of optical properties to polymer along with trying to find new ways to polybutadiene recycling might be considered as presented in the article.

2. Experimental Details

2.1. Materials. Ethylenediamine (EDA), toluene diisocyanate (TDI, colorless liquid, 174.2 g/mol molar mass, 21.8°C melting point, and 48%wt NCO content), dibutyltin dilaurate

(DBTDL), sodium borohydride ($NaBH_4$), urea, citric acid, acetic acid, and periodic acid were all provided by Merck (Germany), and the latter stayed in oven for 2 hours at 80°C before each use to eliminate probable adsorbed moisture. Polybutadiene (average M.N. 5000 g/mol, containing microstructures of 20% 1,2-vinyl, 80% cis-1,4 and trans-1,4.) and also metachloroperbenzoic acid (m-CPBA) were purchased from Sigma Aldrich (USA). Deionized water was received commercially. All solvents were first of all distilled to remove impurities, then fully dried using molecular sieve before use.

2.2. Synthesis of Telechelic Amine Functionalized Polybutadiene. Telechelic aldehyde-functionalized polybutadiene (Ald) preparation advanced by information derived from our recent report (Figure S1) [16]. Synthesized Ald procedure 1.36 mmol (3.42 g) dissolved in dry THF solvent and introduced directly into a glass flask. Under reflux circumstance, the amination of telechelic aldehyde groups of polymer started with EDA 2.04 mmol (0.122 g) addition into the solution and the reaction proceeded for 2 hours in 60°C. It should be noted here that EDA may emit dangerous fumes in the environment. That is why it should be weighed immediately after taking out from the refrigerator and added to the solution mixture. Reduction of ammonium ion intermediate completed through an overnight reaction using $NaBH_4$ 0.5 mmol (0.019 g) and acetic acid 0.82 mmol (47 μL). To avoid instant reaction of acetic acid with $NaBH_4$ and diffusion of unwanted vapors in the reaction pot, the acetic acid should be injected to the solution after $NaBH_4$ total mixing in high-speed stirring (1 min, 1000 rpm). Light yellow amine functionalized polybutadiene product (Am) washed with ethanol several times, after solvent evaporation to eliminate probable residuals and dried completely for 2 days in a vacuum oven in 50°C.

2.3. Synthesis of NGQD Nanoparticles. To prepare N-doped graphene quantum dot (NGQD) from hydrothermal process, a solution containing crystalline citric acid (0.21 g) and urea (0.18 g) dissolved in deionized water (5 ml) was placed in an autoclave internal chamber at 200°C for 4 hours, and the black deposit was obtained (Figure 1). The solution was centrifuged after addition of ethanol. The product was dissolved in deionized water and dried on a glass plate at room temperature for one day.

2.4. Synthesis of Polyurea-NGQD Nanocomposite Films. The synthesized Am 1 mmol (1.2 g) solution in the dry CH_2Cl_2 solvent was poured into a round glass flask. Precise amounts of recent synthesized NGQD nanoparticles (1 and 3 wt%) were added to the solution and exposed to ultrasonic radiation for 30 min. TDI 2 mmol (300 μL) was dissolved in dry CH_2Cl_2 and added dropwise to the reaction mixture. NCO/NH_2 ratios (1 mole Am/2 mole isocyanate) were designed so as to achieve polyurea chains having free isocyanate functional groups at both chain ends (Scheme 2). The reaction followed for 30 min by magnetic stirring, in reflux conditions and 60°C. Finally, the NGQD-PUr nanocomposite synthesis was completed by pouring the crude product into a steel mold and drying in a vacuum oven in 50°C for 1 day.

Figure 1: N-doped graphene quantum dot.

2.5. Characterization. ^{1}H-NMR spectra of the synthesized products were obtained using a Bruker DRX-300 AVANCE instrument (Sweden); chemical shifts appeared in ppm (δ) unit relative to tetramethylsilane (TMS) as the internal standard and deuterated chloroform ($CDCl_3$) as the solvent. FT-IR spectra in 400–4000 cm^{-1} domains were recorded using a Fourier transform Thermo AVATAR infrared spectrophotometer (USA). A thin layer of each sample dissolution in CH_2Cl_2 dry solvent was applied on a blank KBr disc.

A Camspec M350 Double Beam UV-vis instrument (UK) was used and each sample solution in appropriate solvents (chloroform and distilled water based on the nature of the sample) was poured into a zero-absorbance cell of the instrument to record UV-vis absorbances. Photoluminescence emissions of samples transcripted applying 30–40 nm blue-shift based on UV-vis absorbance in a Hitachi (Japan) PL instrument.

TG/DTG thermograms of polyurea and nanocomposites were investigated using a Perkin-Elmer Paris Diamond thermogravimetric analysis instrument (USA), 0–800°C temperature domains, under N_2/O_2 atmosphere and heating rate of 7.5°C/min. Another thermal characteristic analysis of polyurea and nanocomposites was performed using a TA SDT Q600 DSC instrument (USA), temperature range of −100 to 250 was applied at a heating rate of 10°C/min.

The scanning electron microscopy (SEM) technique (TESCAM MIRA III, Czech) was employed for taking SEM pictures, and also energy dispersive X-ray (EDX-mapping) characterizations, in order to perform morphology, dispersion, and nanoparticle size investigations as well as quantitative element identification and abundance studies. AFM pictures taken on a BRUKER ICON (USA) instrument with applying gates of 1, 5, and 10 μm in room temperature.

3. Results and Discussion

3.1. ^{1}H-NMR Spectroscopy. Figure 2 shows the ^{1}H-NMR spectra of Am and PUr samples. The broadened multiple proton peaks below 2.2 ppm are referred to CH_2 groups of

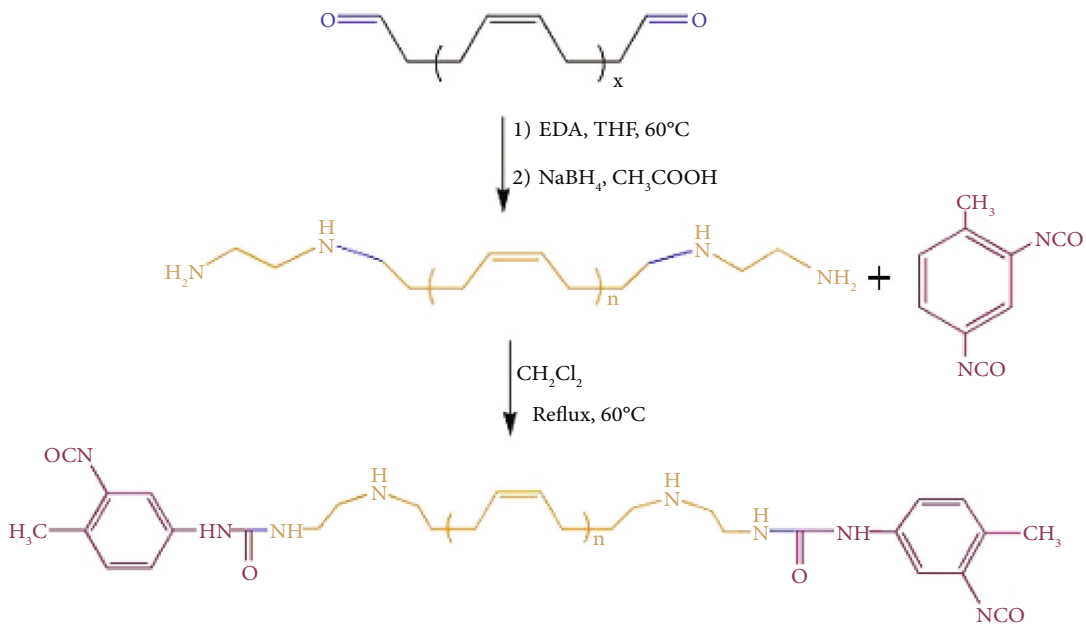

Scheme 2: Synthesis of polyurea film.

the PB chain. Also, *cis*, *trans*, and *vinyl* proton peaks of PB backbone emerged in the 4.8–5.8 ppm region. These patterns are reserved in PUr as well as the Am spectrum. Three different N–CH_2 proton peaks are observed in 2.68, 3.63, and 3.78 ppm. Flattened amine proton peaks are incorporated in 3.05 and 4.24 ppm with weaker integrals in comparison with others. No starting aldehyde polymer indicating proton peak reappeared in 9.8 ppm as residuals of the reaction (Figure S2) [16].

According to PUr spectrum, peaks in 2.67, 3.63, and 3.78 ppm are related to N–CH_2 protons. Also, amine proton peak is indicated at 4.19 ppm. Aromatic diisocyanate protons are traced in 7.06, 1.09, and 7.14 ppm. Weak peaks at 7.65 and 7.78 ppm indicate N–H protons of urea linkage [27].

3.2. FT-IR Spectroscopy. Based on the FT-IR spectrum of Am represented in Figure 3(a), the absorption bands at 3445 and 3338 cm^{-1} are associated with nonsymmetric and symmetric stretching vibrations of 1° and 2° amine N–H bonds. Also, the bending vibration of these bonds is incorporated in the absorption band at 1636 cm^{-1}. The C–N groups are shown by the absorption bands at 1068, 1114, and 1188 cm^{-1} for stretching and band at 1390 cm^{-1} for bending vibrations. Absorption band at 690 cm^{-1} is referred to as N–H group wag vibrations that are only detectable in 1° and 2° types of amines. No absorption bands of the remaining aldehyde procedure are identified (Figure S3).

PUr synthesis approval is depicted in Figure 3(b) utilizing FT-IR spectra. The absorption bands related to the stretching vibrations of free and hydrogen bonded N–H groups are, respectively, recorded at 3442 and 3331 cm^{-1}. Absorption band at 2350 cm^{-1} is associated with stretching vibrations of telechelic free isocyanate functional groups. C=O stretching vibrations of the PUr chain are incorporated in absorption bands at 1631 and 1703 cm^{-1}, respectively, for hydrogen bonded and free carbonyl groups. Aromatic ring breathing absorption band is detected at 1454 cm^{-1}. Absorption band at 1385 cm^{-1} is related to the C–N moieties stretching vibrations, and bands at 1045, 1115, and 1184 cm^{-1} are recorded for bending vibrations of mentioned bonds. It can be realized from both FT-IR and ^{1}H-NMR that correct synthesis of amine functionalized polymer and polyurea is completely provided [27–29].

FT-IR spectra of the NGQD nanoparticle and the PUr-NGQD nanocomposite are plotted in Figure 4. C–N absorption band at 1385 cm^{-1} is emerged because of successful synthesis of NGQD nanoparticles (Figure S4). Amine N–H stretching vibrations collaborated in the formation of absorption bands at 3207 and 3267 cm^{-1} for nanocomposite as well as 3337 and 3408 cm^{-1} in equivalent NGQD which are intensified with O–H absorption of citric acid carboxylic group remained on the GQD. Absorption band at 1736 cm^{-1} C=O is also observed as a result of the presence of carboxylic group. Absorption bands at 1034 and 1101 cm^{-1} related to the bending vibrations of C–N bonds are exactly repeated in the PUr-NGQD spectrum, indicating the presence of N atom in both substances.

The NCO absorption band at 2350 cm^{-1} is vanished in PUr-NGQD in comparison with pure PUr. On the one hand, there were excess amounts of TDI used during the polyurea synthesis approach to maintain telechelic unreacted isocyanate groups. On the other hand, there are carboxyl groups present on GQD that can react with NCO group of polyurea resulting in anhydrides. Besides, based on the literature, some of the doped N atoms are in the N–H from because of the synthesis of NGQD in the water solvent. The N–H can also react with the free isocyanate to make urea groups. So, the NGQD is composited with

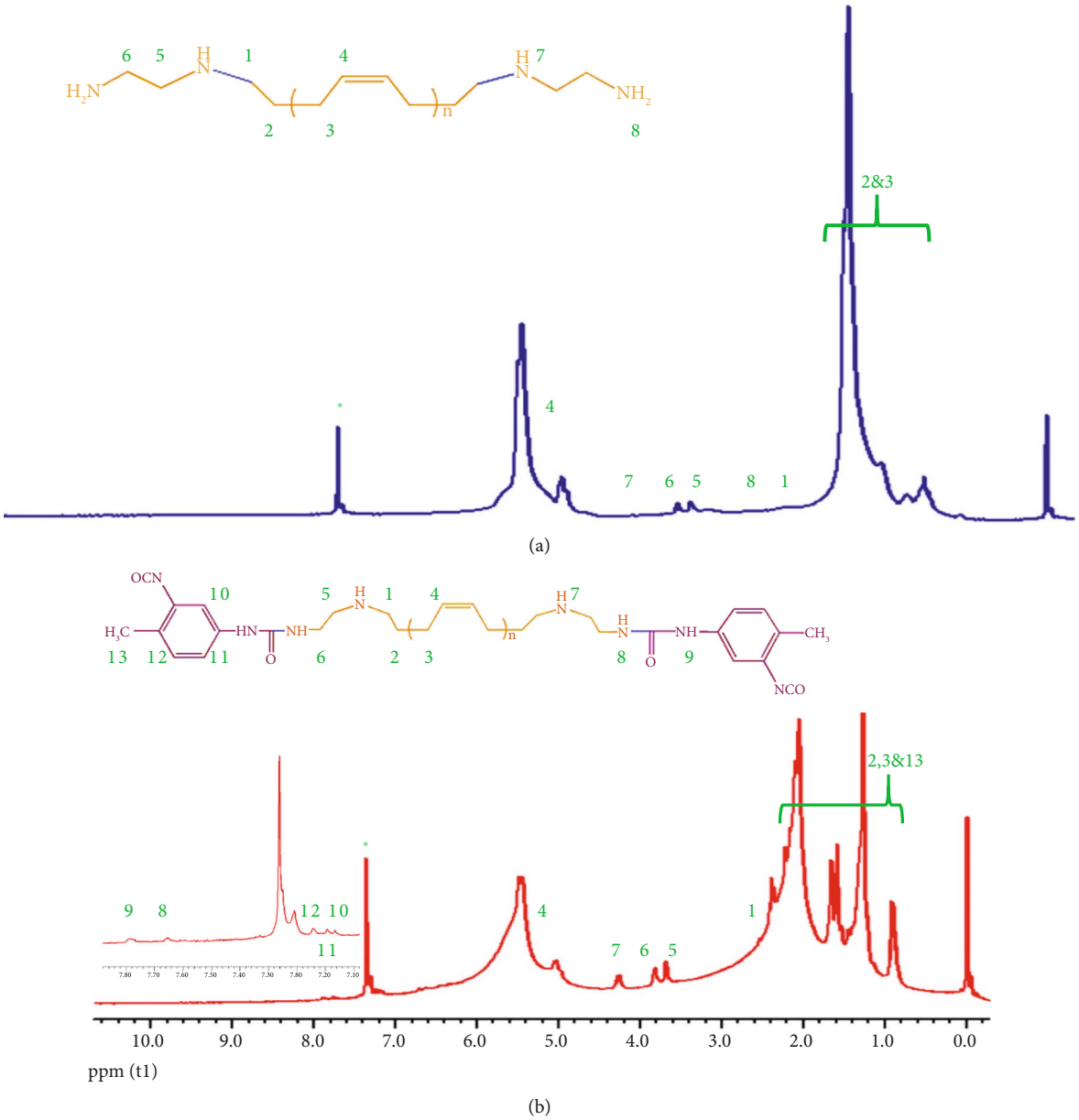

Figure 2: ^{1}H-NMR spectra for stepwise synthesis of PUr. (a) Am and (b) PUr ($^{*}CDCl_3$ solvent peak).

polymer chain using chemical bonds consuming free NCO groups of PUr (Figure 5). Hence, subsidence in carbonyl stretching vibration absorption, slight red shift of this band, and also aromatic C–N bending vibration detection at 1285 cm^{-1} completely approve successful dispersion of nanoparticle in polymer matrix, urea linkage formation, and successful nanocomposite synthesis [30, 31].

3.3. EDX-Mapping. Energy dispersive X-ray analysis and SEM results of nanoparticles are shown, respectively, in Figures 6(a) and 6(b). According to the plot, there are C, O and N elements present in nanoparticle composition. Also, element abundances are shown in Figures 6(c)–6(e). N atom detection proved successful NGQD synthesis.

NGQD nanoparticle EDX data are summarized in Table 1. Based on these results, the C element of the NGQD texture and the O atoms of the remaining citric acid carboxyl groups constitute the majority of nanoparticle composition. 17% of the graphene quantum dot surface is doped with nitrogen element that can play an inevitable role in compositing process, effective interactions of nanoparticles with polymer, and improved characteristics of nanocomposite [32].

3.4. UV-vis Analysis. The UV-vis spectra of NGQD and PUr-NGQD are presented in Figure 7. The strong absorbance at 207.84 nm is related to π–π^{*} electron transfer of C=C bond in graphene structure, which shows a slight blue-shift in comparison with corresponding peak in undoped GQD spectrum reported in literature. The blue-shift can be recognized as the result of nitrogen atom introduction in GQD structure and higher electron affinity of

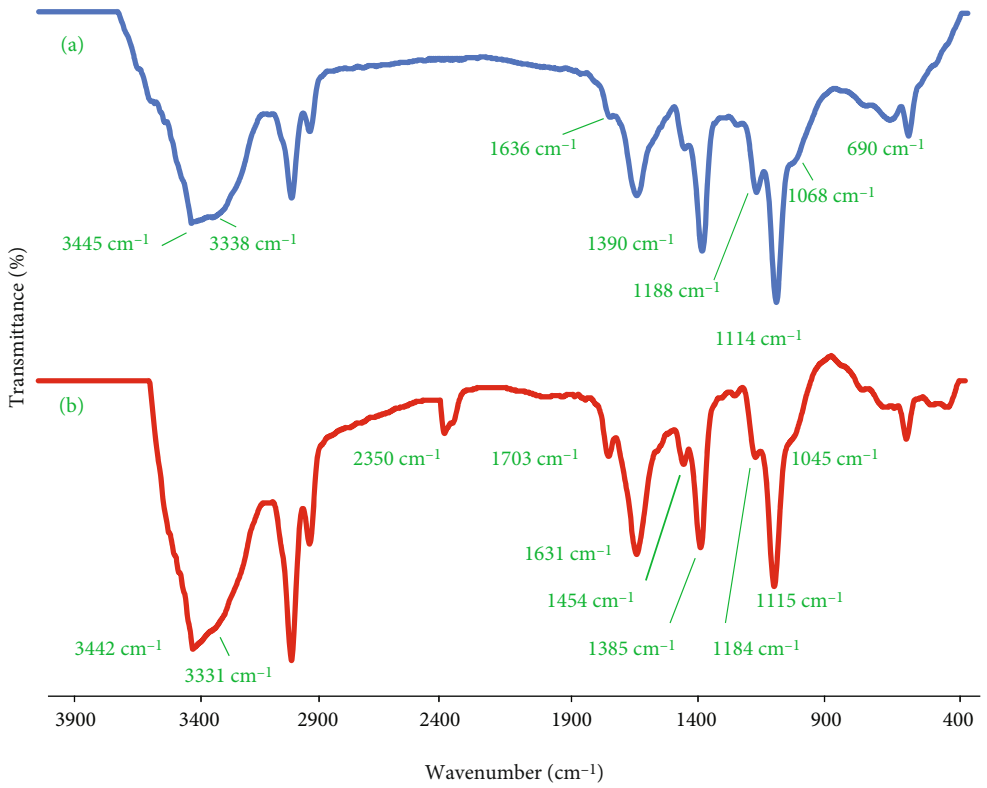

Figure 3: FT-IR spectra for stepwise synthesis of PUr. (a) Am and (b) PUr.

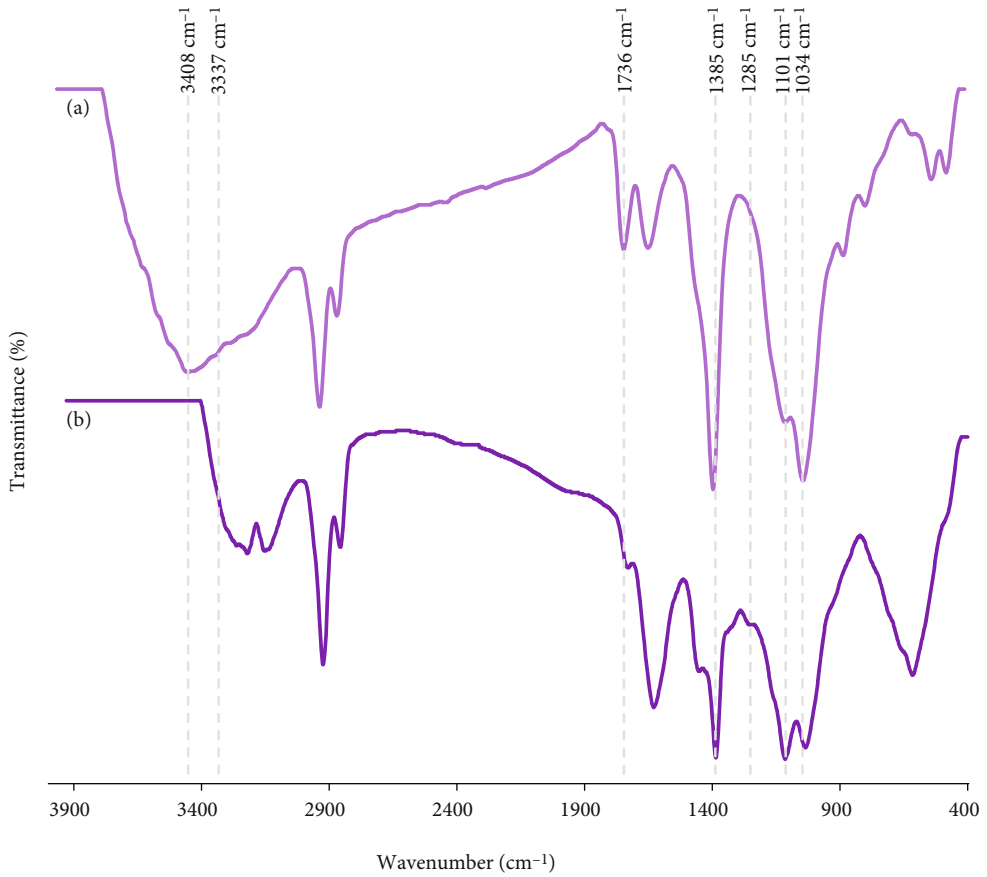

Figure 4: FT-IR spectra. (a) NGQD and (b) PUr-NGQD.

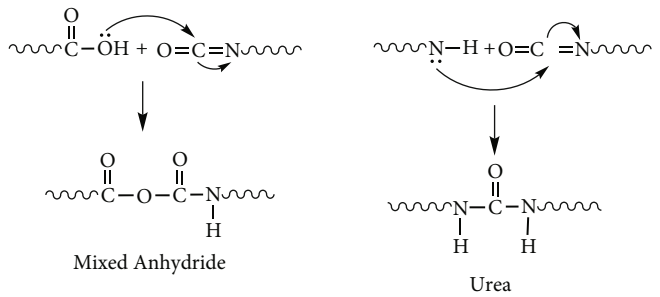

Figure 5: The reaction between free isocyanate of polymer chain with functional groups on NGQD.

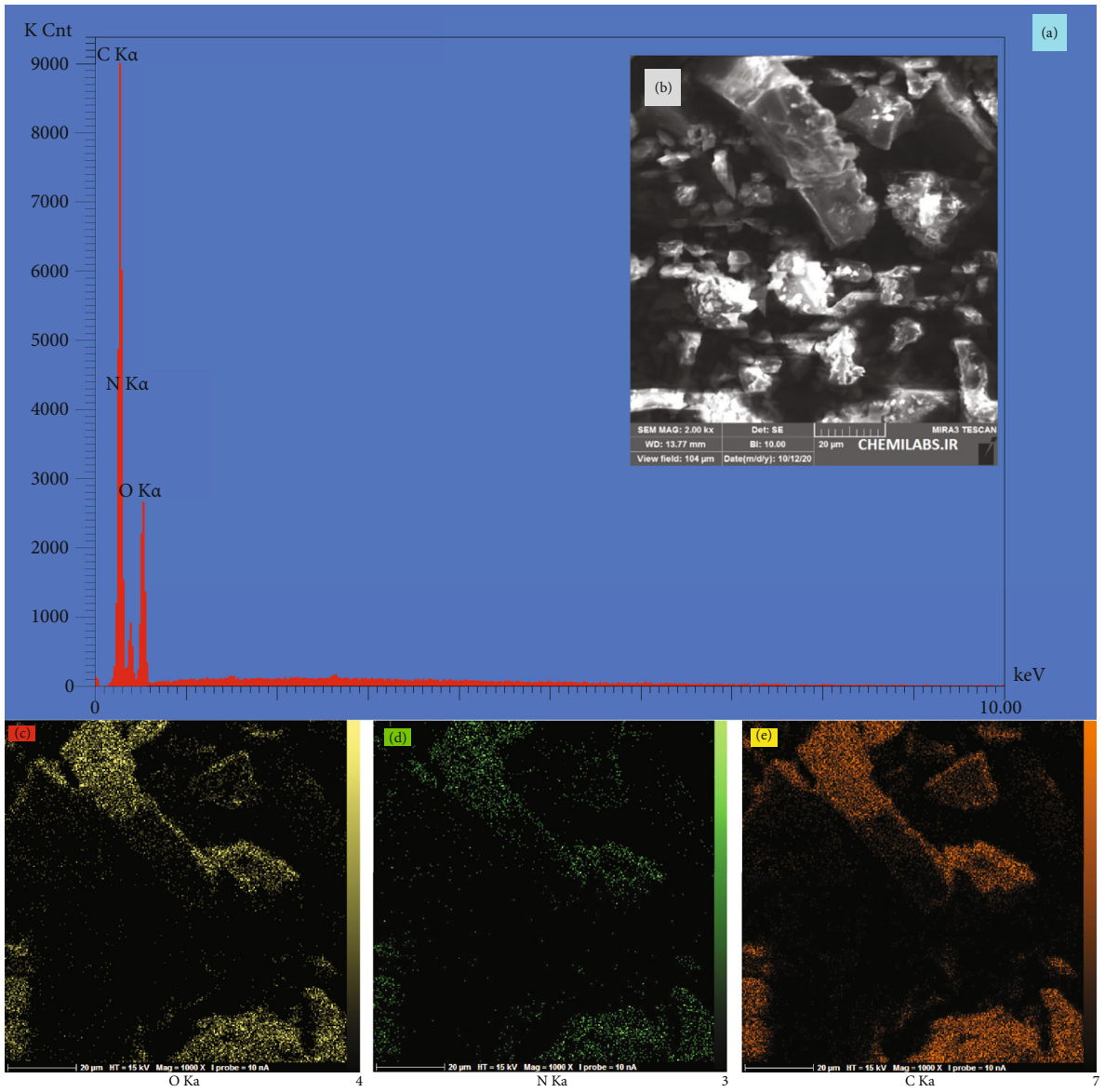

Figure 6: EDX-mapping pictures of NGQD nanoparticle. (a) EDX diffraction pattern of nanoparticle, (b) SEM image of nanoparticle 2 kx magnification, (c) abundance image of C element, (d) abundance image of N element, and (e) abundance image of O element.

this atom. The peaks at 254.48, 278.02, and 423.35 nm are, respectively, recorded for n–π^* electron transfer in C=O bond, n–π^* electron transfer in C=N bond and absorbance of nanoscale particles (Figure 7(a)) [33, 34].

The major absorbance of PUr-NGQD (Figure 7(b)) emerged at 254.15 nm with 46 nm red-shift in comparison with NGQD nanoparticles. The red-shift could be considered as the consequence of NGQD interaction with the PUr chain, the band

Table 1: EDX plot data summery of NGQD nanoparticle.

Element	Atom percentage (%)	Weight (%)
Carbon	46.36	40.34
Oxygen	36.19	41.95
Nitrogen	17.45	17.71

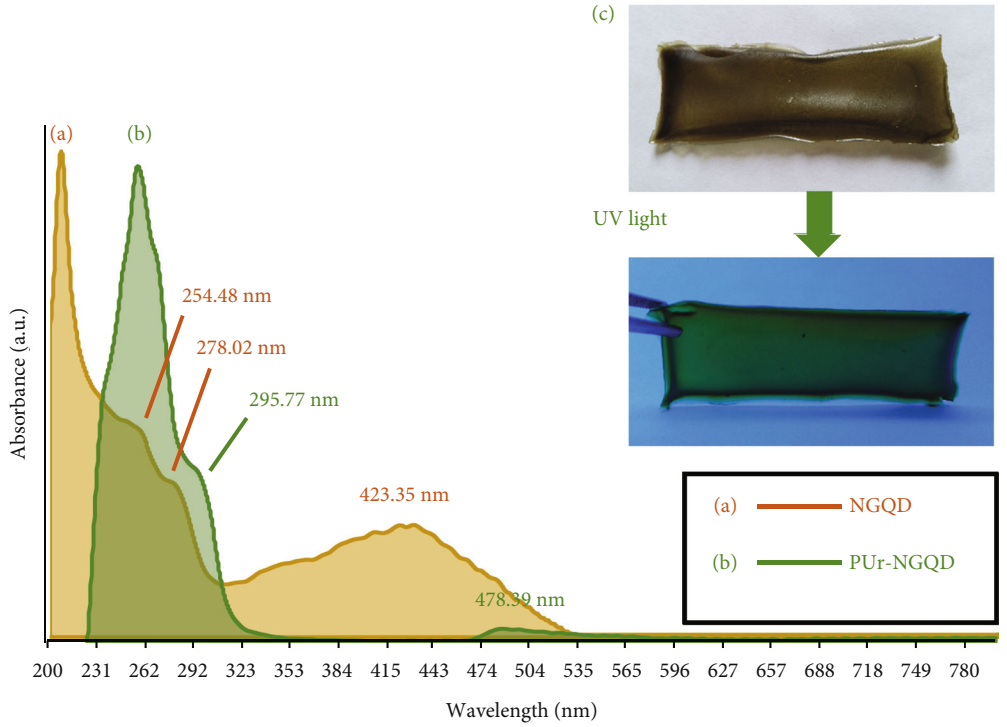

Figure 7: UV-vis spectra. (a) NGQD, (b) PUr-NGQD, and (c) PUr-NGQD image in UV light.

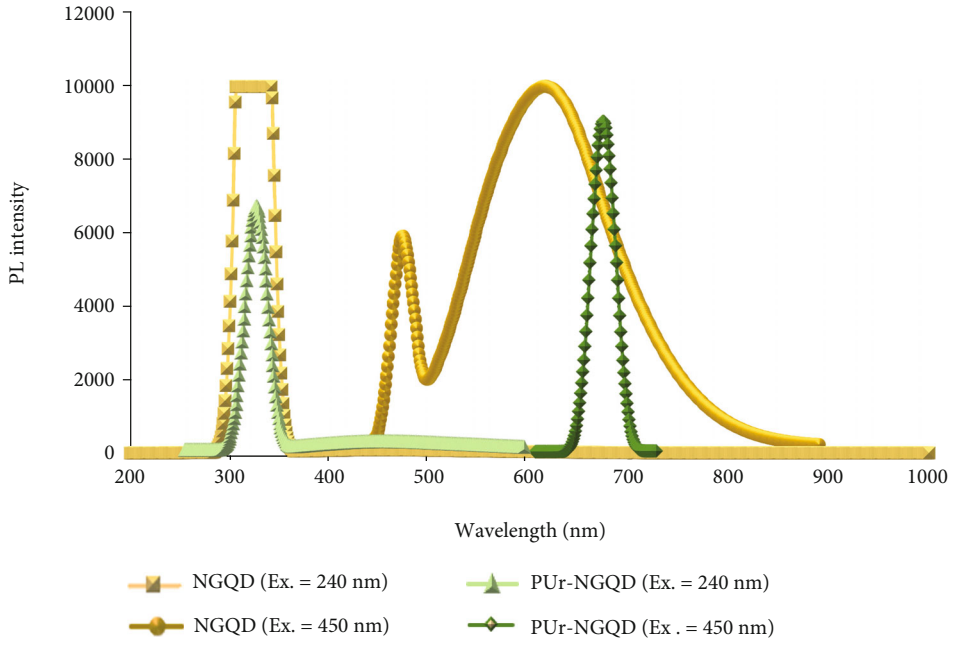

Figure 8: PL spectra of NGQD and PUr-NGQD.

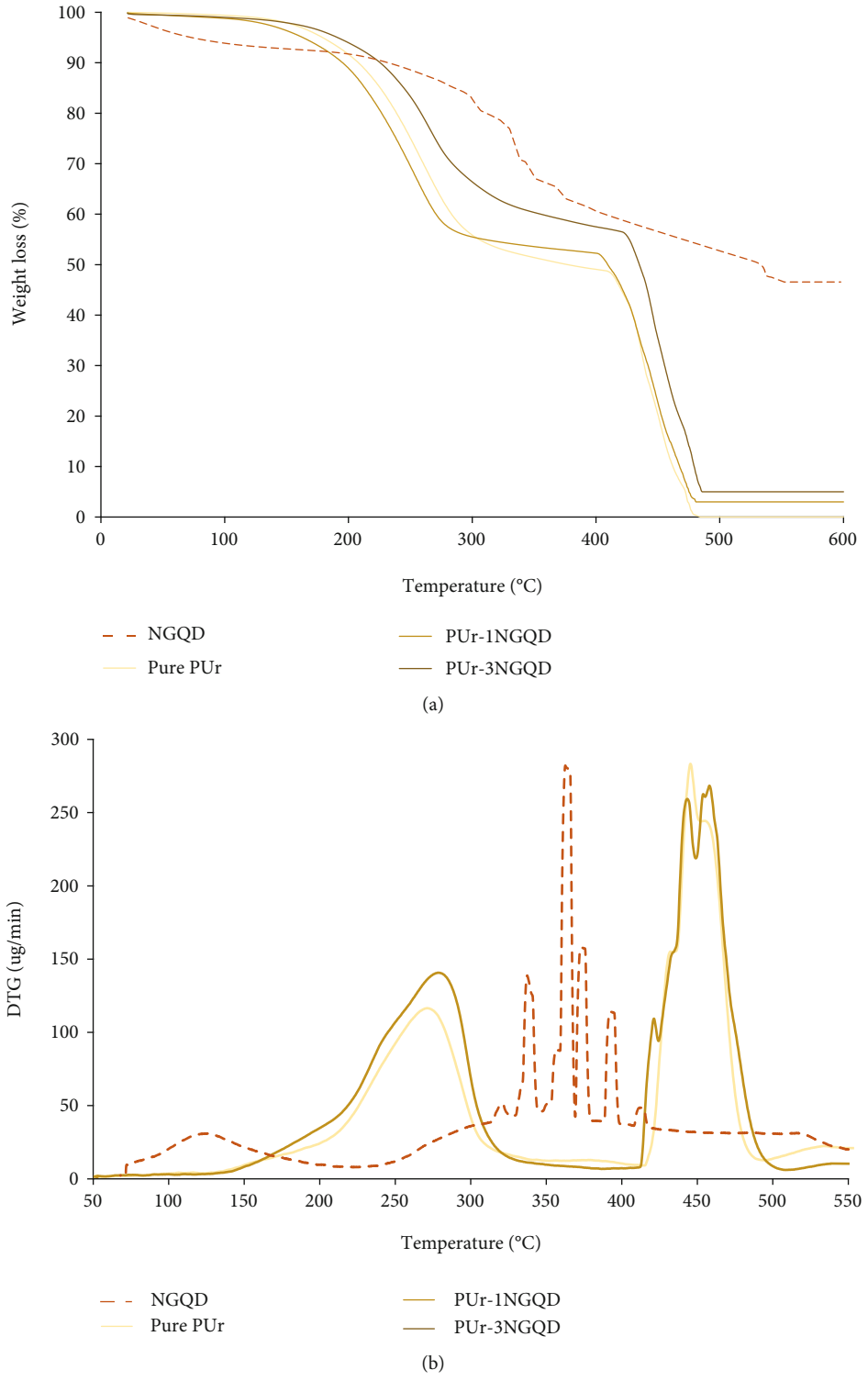

Figure 9: TGA/DTG Thermograms of NGQD nanoparticle, pure PUr, and PUr-NGQD nanocomposites.

gap energy decline, and the increase in conjugation length. The UV absorption can vary with the conjugation length. The graphene quantum dot structure is full of conjugated double bonds, and the conjugation length might increase through chemical bond with a polybutadiene-based polyurea with regular double bonds. The election flux raise causes a decline in the band gap energies and leads to higher wavelength absorbances [16].

Table 2: Degradation data of PUr and PUr-NGQD nanocomposites.

Sample	T_O, ˚C	T_{10}, ˚C	T_{50}, ˚C	T_f, ˚C
PUr	199	227	371	475
PUr-1NGQD	205	215	416	483
PUr-3NGQD	211	243	441	491

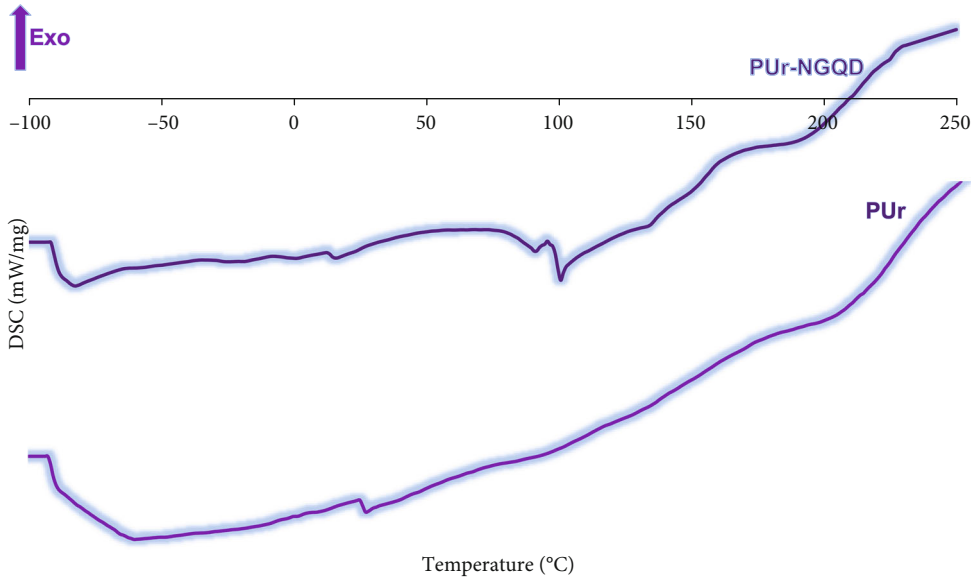

Figure 10: DSC Thermograms of PUr and PUr-NGQD nanocomposites.

Optical properties of the PUr-NGQD nanocomposite remained unchanged without any quenching. Other absorbances are seen at 295.77 and 478.39 nm; the latter one is accompanied with 55 nm red-shift and significant quenching for the reason of homogenous nanoparticle dispersion, in the PUr matrix and successful interactions. Green absorbance of PUr-NGQD nanocomposite is obviously recognizable in Figure 7(c), when exposed to UV light [35, 36].

3.5. PL Analysis. PL emission of NGQD nanoparticles and PUr-NGQD nanocomposite is investigated in different excitation gates (Figure 8). PL emission of the NGQD peak of 324 nm is recorded for an excitation gate of 240 nm, and two distinct emissions of 469 and 624 nm are observed for 450 nm of excitation. Emissions of 323 and 662 nm are, respectively, observed as a result of 240 and 450 nm excitation gates applied to PUr-NGQD [37].

Emission peaks of PUr-NGQD appeared with narrower bandwidth than NGQD. Like any other nanoparticles with particle size below 50 nm, NGQD species tend to assemble in pure state, raise in particle size and emit in thicker peaks. During compositing with PUr matrix, the probability of agglomeration eliminates and particle size of NGQD in nanocomposite are smaller than the non-composited ones. The smaller the NGQD particle size, the narrower the PL peak bandwidth.

No obvious quenching has occurred that can disturb optical properties of nanocomposite. However, the quenching of nanocomposite emission in primary excitation could be visualized because of homogeneous distribution of nanoparticles in the polymer matrix that accelerated the electron transfer through energy levels. Strong interactions between PUr chain and the N atom of NGQD could contributed to the second excitation red shift. These excitations and longer emissions along with UV-vis results make nanocomposite an ideal component in bioimaging applications [34, 38].

3.6. TGA/DTG Analysis. TGA/DTG thermograms of NGQD nanoparticles, pristine PUr, and PUr-NGQD nanocomposites are plotted in Figure 9. A rule of two-step degradation is reserved in appearance of all four thermograms. 43 weight percent of NGQD nanoparticles remained steady, and it experienced a 53% two-step weight loss until 538°C. After approximately 2% weight loss of probable solvent evaporation and impurity in temperatures of 100–120°C, hard segment degradation of PUr, PUr-1NGQD, and PUr-3NGQD is, respectively, completed with 42%, 41%, and 32% weight loss in 323, 282, and 297°C. Hard segment degradation step in PUr-1NGQD is happened in lower temperatures in comparison with pure PUr. This phenomenon could be observed because of interchain interaction cleavage (microphase separation interruption) as a consequence of nanoparticle entrance and free isocyanate hard segment consumption. It seems that nanoparticle interaction energy was not so strong to compensate for the loss of chain ordering.

The second step related to the soft segment degradation is detected at temperatures of 475, 483, and 491°C, respectively, with 56%, 57%, and 67% weight loss in PUr, PUr-1NGQD, and PUr-3NGQD.

Thermal decomposition data of PUr and PUr-NGQD nanocomposites are summarized in Table 2. It can be extracted from table data that nanocomposites hit higher temperatures than pure PUr in all degradation levels. So, it can be concluded that the nanocomposite entrance in the PUr matrix leads to thermal resistance of nanocomposites by making high-energy interactions.

3.7. DSC Analysis. DSC thermograms of PUr and PUr-NGQD nanocomposite are shown in Figure 10. According to the thermograms of PUr, first glass transition related to the mobility of polybutadiene backbone soft segments is detected in −72°C, while second transition attributed to polyurea hard segments is registered in 24°C with a specific heat of 0.12 J/g*K. In the same manner, two halts in −85

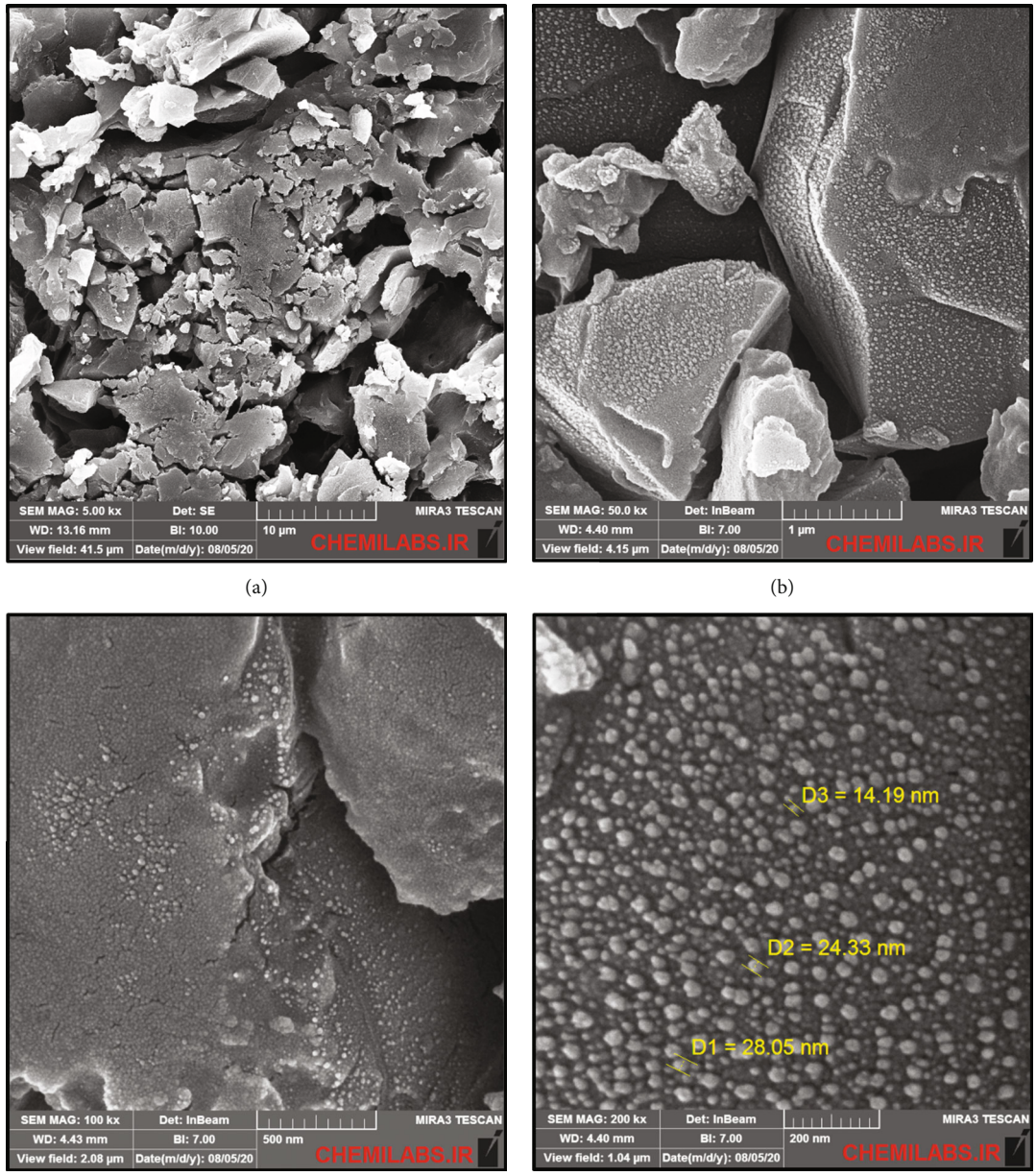

Figure 11: SEM micrographs of PUr-NGQD nanocomposites. (a) ×5000, (b) ×50000, (c) ×100000, and (d) ×201,000.

and 11°C are emerged, respectively, for T_g of soft and hard segments in PUr-NGQD. Both T_gs are observed at 13°C lower than corresponding temperatures in pristine PUr as a consequence of microphase separation caused by nanoparticle interactions with polymer chains and also consuming free isocyanate hard segments [14].

PUr-NGQD melting point is verified at 90°C having enthalpy of 12.71 J/g with 10°C and 7.31 J/g improvement rather than equivalent values in PUr. Degradation process is traced in 203 and 192°C with enthalpy of 1.8 and 1.73 J/g, respectively, in PUr and PUr-NGQD. Despite higher melting data, the bond dissociation and degradation process began at lower temperatures and enthalpies in comparison with PUr. So, thermal characteristic improvement in PUr-NGQD arises from capability of nanoparticles in heat reservation and storage, hence the interactions, although strong, do not have enough energy to delay the onset of the degradation process. However, increasing the melting point and decreasing T_g promise the performance of the nanocomposite over a wider temperature range [39].

3.8. SEM Analysis. Based on Figure 11, the average nanoparticle size in SEM micrographs of PUr-NGQD nanocomposite is designated at 22.19 nm. On the one hand, the existence of particles in the nano range is proved and, on the other hand, the occurrence of any agglomeration of nanoparticles is ruled out. As a result of this homogenous nanoparticle dispersion, the thermal and optical properties of nanocomposite are

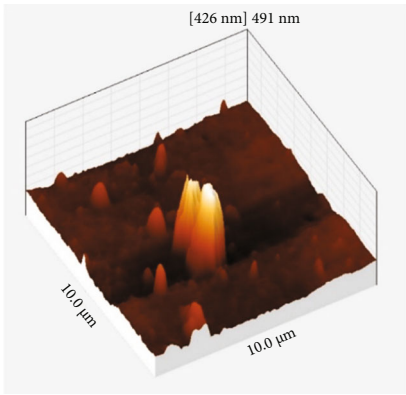

(a)

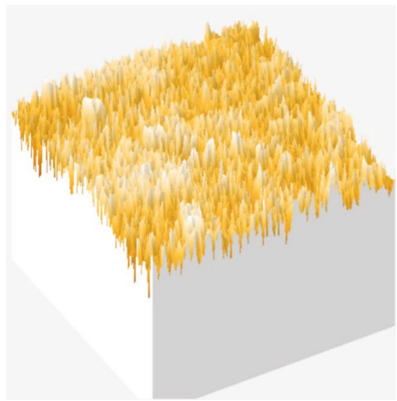

(b)

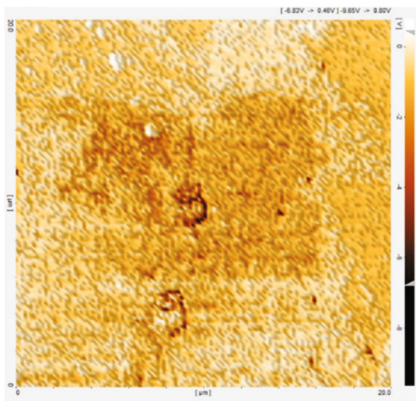

(c)

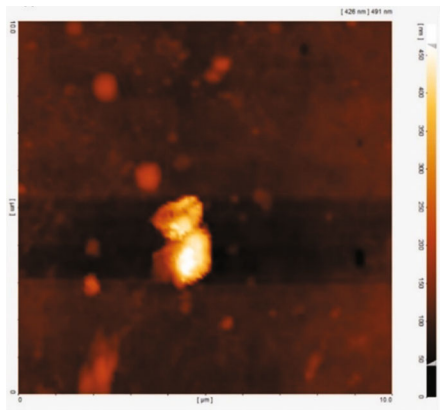

(d)

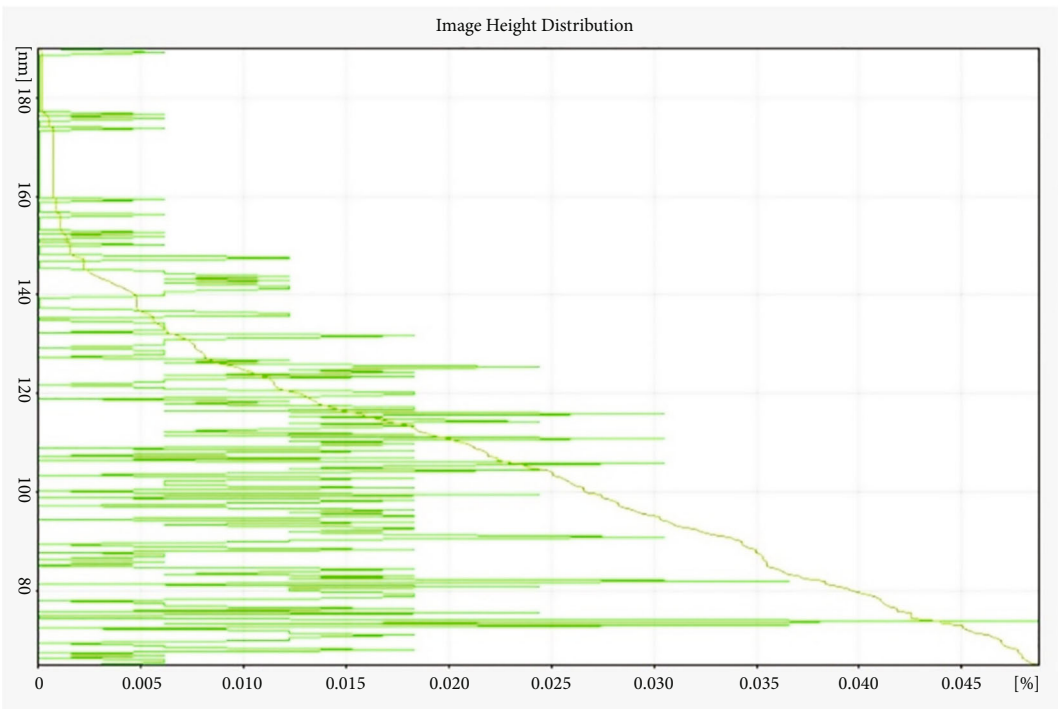

(e)

Figure 12: Continued.

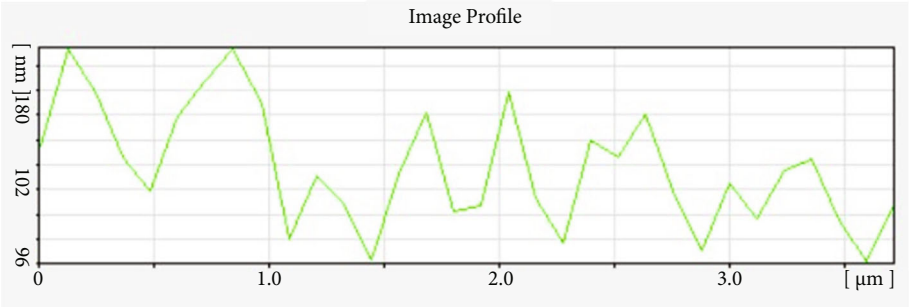

(f)

Figure 12: AFM images of PUr-NGQD: (a) and (b) 3D scheme, (c) and (d) 2D images, (e) height distribution plot, and (f) height profile.

Table 3: AFM analysis data of PUr and PUr-NGQD nanocomposites.

Sample	50% distrib. (nm)	R_a (nm)	R_{max} (nm)	R_{min} (nm)	R_p (nm)	R_v (nm)
PUr	476	1968	2287	1538	333.6	−358.8
PUr-NGQD	80	102	108	92	108.9	−21

50% distrib.: height distribution of 50% of detected surface particles. R_a: average roughness. R_{max}: maximum height profile roughness. R_{min}: minimum height profile roughness. R_p: maximum profile peak height. R_v: maximum profile valley depth.

settled at the desired level from previous parts, which can be due to the excess interactions of the N atom introduced into the nanoparticle [40].

3.9. AFM Analysis. The AFM pictures related to topographic and morphologic investigations of the PUr-NGQD nanocomposite surface are gathered in Figures 12(a)–12(f). Tops and heights and also depths and valleys become visible as the result of instrument needle influence, respectively, on hard and soft segments of the polymer chain [39, 41]. It seems from both 3D schemes of nanocomposite film surface that heights and valleys are more homogeneous and transformed to soft parts in comparison with pristine PUr (Figure S5) [14]. Also, obviously visible dark parts in 2D images obtained by using 10 μm imaging gate are recorded for the presence of nanoparticles in lower size than 50 nm (Figures 12(c) and 12(d)) [42].

Table 3 presents a summary of topographic data statistic evaluation. It resulted from data and picture collection, and outcome comparison with pure PUr that nanocomposite synthesis is successful. Also, NGQD nanoparticle entrance, homogeneous distribution in PUr matrix, and beneficial interactions with chains is consequenced exfoliation, flattening, and order creation on the surface of the nanocomposite. Significant reduction of the roughness, entanglement, and complexity of the soft parts in the polymer chain resulted in a height decrease and a softer surface in comparison with pristine PUr (beside UV-vis and PL results), which make nanocomposite a well featured candidate for usage in optical coatings [43].

4. Conclusion

In this study, the reaction of citric acid with urea was performed through a hydrothermal method in order to synthesize of NGQD nanoparticles. In follow up, the reaction of synthesized polyamine with TDI diisocyanate through an in situ polymerization process was used in the presence of different nanoparticle amounts for PUr-NGQD nanocomposite synthesis. The NGQD nanoparticles and PUr-NGQD nanocomposite synthesis accuracy was investigated by the FT-IR test. Also, N atom presence within NGQD structure characterized using the EDX analysis was an acceptable estimation of successful GQD N-doping. UV-vis and PL studies showed that the optical properties of nanoparticles are maintained in a proper way in nanocomposite. PUr-NGQD nanocomposites showed a slightly better thermal characteristics than pure PUr from TGA/DTG and DSC analysis data interpretation. Finally, successful synthesis of nanocomposite and distribution of nanoparticles and improvement of surface and morphological properties in PUr-NGQD nanocomposite were proved using the SEM and AFM studies. This study introduced an optically active thermal stable nanocomposite obtained from polybutadiene chain functionalization for hopefully opening a window to synthesis of value-added nanocomposites from recycling materials for use in optical active coatings in the near future.

Abbreviations

PB: Polybutadiene
Am: Telechelic amine functionalized polybutadiene
PUr: Polyurea
GQD: Graphene quantum dot
NGQD: Nitrogen-doped graphene quantum dot
PUr-NGQD: Nanocomposite of polyurea with NGQD nanofiller
PUr-1NGQD and PUr-3NGQD: Nanocomposites with, respectively, 1 and 3 weight percent of NGQD nanoparticle in PU matrix
^{1}H-NMR: Proton nuclear magnetic resonance spectroscopy

FT-IR:	Fourier transform-infrared spectroscopy
EDX:	Energy dispersive X-ray analysis
UV-vis:	Ultraviolet–visible spectrophotometry
PL:	Photoluminescence spectroscopy
TGA/DTG:	Thermogravimetric and differential thermogravimetric analysis
DSC:	Differential scanning calorimetry
SEM:	Scanning electron microscopy
AFM:	Atomic force microscopy.

Data Availability

The data used to support the findings of this study are included within the supplementary information file.

Conflicts of Interest

The authors declare that they have no conflicts of interest.

Authors' Contributions

All three authors contributed to the study conception and design. Material preparation, data collection and analysis were performed by Zahra Rahmatpanah. The first draft of the manuscript was written by Zahra Rahmatpanah, Mir Mohammad Alavi and Maryam Dargahi commented on previous versions of the manuscript. All three authors read and approved the final manuscript.

Acknowledgments

The authors would like to thank Imam Khomeini International University (IKIU).

Supplementary Materials

Figure S1 telechelic aldehyde-functionalized polybutadiene (Ald) product image. Figure S2. ^{1}H-NMR spectra. (a) PB, (b) Ald. Figure S3. FT-IR spectra. (a) PB, (b) Ald. Figure S4 FT-IR spectra. (a) Citric acid, (b) GQD. Figure S5 AFM images of PUr: (a) 3D scheme, (b) and (c) 2D images, (d) height histogram, (e) height distribution plot, (f) roughness profile *(Supplementary Materials)*

References

[1] Y. Xiao, H. Zou, L. Zhang, X. Ye, and D. Han, "Surface modification of silica nanoparticles by a polyoxyethylene sorbitan and silane coupling agent to prepare high-performance rubber composites," *Polymer Testing*, vol. 81, article 106195, 2020.

[2] L. M. Polgar, M. Van Duin, A. Broekhuis, and F. Picchioni, "Use of Diels-Alder chemistry for Thermoreversible crosslinking of rubbers: the next step toward recycling of rubber products?," *Macromolecules*, vol. 48, no. 19, pp. 7096–7105, 2015.

[3] T.-C. Chiang, H.-L. Liu, L.-C. Tsai, T. Jiang, N. Ma, and F.-C. Tsai, "Improvement of the mechanical property and thermal stability of polypropylene/recycled rubber composite by chemical modification and physical blending," *Scientific Reports*, vol. 10, no. 1, p. 2432, 2020.

[4] Y. Fang, M. Zhan, and Y. Wang, "The status of recycling of waste rubber," *Materials and Design*, vol. 22, no. 2, pp. 123–128, 2001.

[5] J. Bai, H. Li, Z. Shi, and J. Yin, "An eco-friendly scheme for the cross-linked polybutadiene elastomer via thiol-Ene and Diels-Alder click chemistry," *Macromolecules*, vol. 48, no. 11, pp. 3539–3546, 2015.

[6] E. Trovatti, T. M. Lacerda, A. J. F. Carvalho, and A. Gandini, "Recycling tires? Reversible crosslinking of poly(butadiene)," *Advanced Materials*, vol. 27, pp. 1–4, 2015.

[7] M. M. A. Nikje and H. Hajifatheali, "Performance of dimethyl dioxirane/nano-TiO_2 on epoxidation of polybutadiene and hydroxyl terminated polybutadiene," *Journal of Elastomers and Plastics*, vol. 45, no. 5, pp. 457–469, 2013.

[8] P. Berto, S. Grelier, and F. Peruch, "Telechelic polybutadienes or Polyisoprenes precursors for recyclable elastomeric networks," *Macromolecules*, vol. 38, pp. 2–7, 2017.

[9] M. Amiri, M. Salavati-Niasari, A. Pardakhty, M. Ahmadi, and A. Akbari, "Caffeine: a novel green precursor for synthesis of magnetic $CoFe_2O_4$ nanoparticles and pH-sensitive magnetic alginate beads for drug delivery," *Materials Science and Engineering C*, vol. 76, pp. 1085–1093, 2017.

[10] J. Quagliano, J. Bocchio, and P. Ross, "Mechanical and swelling properties of hydroxyl-terminated polybutadiene-based polyurethane elastomers," *The Minerals, Metals & Materials Society*, vol. 71, no. 6, pp. 2097–2102, 2019.

[11] Q. Zhou, S. Jie, and B. G. Li, "Facile synthesis of novel HTPBs and EHTPBs with high cis-1,4 content and extremely low glass transition temperature," *Polymer*, vol. 67, pp. 208–215, 2015.

[12] G. Morandi, N. Kebir, I. Campistron, F. Gohier, A. Laguerre, and J. F. Pilard, "Direct selective reductive amination of carbonyl telechelic oligoisoprenes: elaboration of promising tri- and tetrafunctionalized oligoisoprene intermediates," *Tetrahedron Letters*, vol. 48, no. 43, pp. 7726–7730, 2007.

[13] P. Phinyocheep, C. W. Phetphaisit, D. Derouet, I. Campistron, and J. C. Brosse, "Chemical degradation of epoxidized natural rubber using periodic acid: preparation of epoxidized liquid natural rubber," *Applied Polymer Science*, vol. 95, no. 1, pp. 6–15, 2005.

[14] Z. Rahmatpanah and M. M. A. Nikje, "Synthesis and characterization of thermally stable polyurea-TiO_2 nanocomposites based on amine terminated polybutadiene," *Polymer Bulletin*, vol. 80, 2022.

[15] N. Kebir, I. Campistron, A. Laguerre et al., "Use of hydroxytelechelic cis-1,4-polyisoprene (HTPI) in the synthesis of polyurethanes (PUs). Part 1. Influence of molecular weight and chemical modification of HTPI on the mechanical and thermal properties of PUs," *Polymer*, vol. 46, no. 18, pp. 6869–6877, 2005.

[16] Z. Rahmatpanah and M. M. A. Nikje, "A novel synthesis of polybutadiene-based polyurethane binder and conductive graphene–polyurethane nanocomposites: a new approach to polybutadiene recycling," *Polymer Bulletin*, vol. 78, pp. 3651–3666, 2020.

[17] P. Berto, A. Pointet, C. L. Coz, S. Grelier, and F. Peruch, "Recyclable Telechelic cross linked polybutadiene based on reversible Diels–Alder chemistry," *Macromolecules*, vol. 51, pp. 651–659, 2017.

[18] S. P. Jovanovic, Z. Syrgiannis, Z. Markovic et al., "Modification of structural and luminescence properties of graphene quantum dots by gamma irradiation and their application in a photodynamic therapy," *ACS Applied Materials & Interfaces*, vol. 7, no. 46, pp. 25865–25874, 2015.

[19] S. Singh, G. L. Dhakar, B. P. Kapgate et al., "Synthesis and chemical modification of crystalline nanocellulose to reinforce natural rubber composites," *Polymers for Advanced Technologies*, vol. 31, no. 12, pp. 3059–3069, 2020.

[20] D. Bera, L. Qian, T. K. Tseng, and P. H. Holloway, "Quantum dots and their multimodal applications: a review," *Materials*, vol. 3, no. 4, pp. 2260–2345, 2010.

[21] S. P. Moghanlo and H. Valizadeh, "Microwave-assisted preparation of graphene quantum dots immobilized nanosilica as an efficient heterogeneous nanocatalyst for the synthesis of xanthenes," *Organic Communications*, vol. 12, no. 1, pp. 14–25, 2019.

[22] L. Tang, R. Ji, X. Li et al., "Deep ultraviolet to near-infrared emission and Photoresponse in layered N-doped graphene quantum dots," *ACS Nano*, vol. 8, no. 6, pp. 6312–6320, 2014.

[23] M. Kaur, M. Kaur, and V. K. Sharma, "Nitrogen-doped graphene and graphene quantum dots: a review onsynthesis and applications in energy, sensors and environment," *Advances in Colloid and Interface Science*, vol. 259, pp. 44–64, 2018.

[24] C. Hu, Y. Liu, Y. Yang et al., "One-step preparation of nitrogen-doped graphene quantum dots from oxidized debris of graphene oxide," *Journal of Materials Chemistry B*, vol. 8, pp. 39–42, 2013.

[25] Z. Rahmatpanah and M. M. A. Nikje, "Thermally stable magnetic polyurethane nanocomposites prepared from functionalized polybutadiene: novel approach to the polybutadiene chemical modification," *Russian Journal of Applied Chemistry*, vol. 94, no. 6, pp. 835–845, 2021.

[26] Z. Rahmatpanah, M. M. A. Nikje, and M. Dargahi, "Optical active thermal stable nanocomposites using polybutadiene-based polyurethane and graphene quantum dot-MnO_2," *International Journal of Polymer Science*, vol. 2022, 2022.

[27] C. Wu, J. Wang, P. Chang et al., "Polyureas from diamines and carbon dioxide: synthesis, structures and properties," *Physical Chemistry Chemical Physics*, vol. 14, no. 2, pp. 464–468, 2012.

[28] A. Bahadur, A. Saeed, S. Iqbal et al., "Biocompatible waterborne polyurethane-urea elastomer as intelligent anticancer drug release matrix: a sustained drug release study," *Reactive and Functional Polymers*, vol. 119, pp. 57–63, 2017.

[29] W. Liu, C. Fang, F. Chen, and X. Qiu, "Strong, reusable, and self-healing lignin-containing polyurea adhesives," *ChemSusChem*, vol. 17, no. 17, pp. 1–11, 2020.

[30] P. Pimpang, R. Sumang, and S. Choopun, "Effect of concentration of citric acid on size and optical properties of fluorescence graphene quantum dots prepared by tuning carbonization degree," *Chiang Mai Journal of Science*, vol. 45, pp. 2005–2014, 2018, https://www.researchgate.net/publication.

[31] J. Lu, Y. Kou, X. Jiang et al., "One-step preparation of poly(-glyoxal-bis(2-hydroxyanil))-amino-functionalized graphene quantum dots-MnO_2 composite on electrode surface for simultaneous determination of vitamin B2 and dopamine," *Colloids and Surfaces A*, vol. 580, article 123652, 2019.

[32] R. Monsef, M. Ghiyasiyan-Arani, and M. Salavati-Niasari, "Design of magnetically recyclable ternary Fe_2O_3/$EuVO_4$/g-C_3N_4 nanocomposites for photocatalytic and electrochemical hydrogen storage," *ACS Applied Energy Materials*, vol. 4, no. 1, pp. 680–695, 2021.

[33] V. Melinte, T. Buruiana, I. D. Moraru, and E. C. Buruiana, "Silver-polymer composite materials with antibacterial properties," *Digest Journal of Nanomaterials and Biostructures*, vol. 6, pp. 213–223, 2011, https://www.researchgate.net/publication.

[34] J. Ju and W. Chen, "Synthesis of highly fluorescent nitrogen-doped graphene quantum dots for sensitive, label-free detection of Fe(III) in aqueous media," *Biosensors and Bioelectronics*, vol. 58, pp. 219–225, 2014.

[35] R. Duarah and N. Karak, "High performing smart hyperbranched polyurethane nanocomposites with efficient self-healing, self-cleaning and photocatalytic attributes," *New Journal of Chemistry*, vol. 42, pp. 2167–2179, 2017.

[36] L. Jing, H. L. Tan, R. Amal, Y. H. Ng, and K. N. Sun, "Polyurethane sponge facilitating highly dispersed TiO_2 nanoparticles on reduced graphene oxide sheets for enhanced photoelectro-oxidation of ethanol," *Journal of Materials Chemistry A*, vol. 3, no. 30, pp. 15675–15682, 2015.

[37] F. Davar, M. Salavati-Niasari, and Z. Fereshteh, "Synthesis and characterization of SnO_2 nanoparticles by thermal decomposition of new inorganic precursor," *Journal of Alloys and Compounds*, vol. 496, no. 1–2, pp. 638–643, 2010.

[38] Y. F. Zhang, Y. H. Zhao, S. L. Bai, and X. Yuan, "Numerical simulation of thermal conductivity of graphene filled polymer composites," *Composites Part B Engineering*, vol. 106, pp. 324–331, 2016.

[39] Y. Cai, J.-S. Jiang, B. Zheng, and M.-R. Xie, "Synthesis and properties of magnetic sensitive shape memory Fe_3O_4/poly(e-caprolactone)-polyurethane nanocomposites," *Applied Polymer Science*, vol. 127, pp. 1–8, 2012.

[40] S. Ahmadian-Fard-Fini, D. Ghanbari, O. Amiri, and M. Salavati-Niasari, "Electro-spinning of cellulose acetate nanofibers/Fe/carbon dot as photoluminescence sensor for mercury (II) and lead (II) ions," *Carbohydrate Polymers*, vol. 229, article 115428, 2020.

[41] S. Gomez-Fernandez, L. Ugarte, C. Pena-Rodriguez, M. Zubitur, M. A. Corcuera, and A. Eceiza, "Flexible polyurethane foam nanocomposites with modified layered double hydroxides," *Applied Clay Science*, vol. 123, pp. 109–120, 2016.

[42] P. Ross, G. Escobar, G. Sevilla, and J. Quagliano, "Micro and nanocomposites of polybutadienebased polyurethane liners with mineral fillers and nanoclay: thermal and mechanical properties," *Open Chemistry*, vol. 15, no. 1, pp. 46–52, 2017.

[43] N. Kebir, I. Campistron, A. Laguerre, J. F. Pilard, and C. Bunel, "New crosslinked polyurethane elastomers with various physical properties from natural rubber derivatives," *Applied Polymer Science*, vol. 122, no. 3, pp. 1677–1687, 2011.